Industrial Applications of Nonlinear Modal Modeling: Two Case Studies

Benjamin R Pacini
Sandia National Laboratories†
P.O. Box 5800 – MS0557
Albuquerque, NM, 87185

Abstract
Nonlinear structural dynamics testing, identification and modeling is becoming increasingly popular. While many methods exist, the focus of this work is nonlinear modal modeling, a framework for capturing the nonlinear behavior of a structure on a mode-by-mode basis by augmenting a linear modal model with amplitude-dependent stiffness and damping elements placed in parallel with their linear counterparts. Once identified, this highly reduced order model can be used to simulate and predict the response of a structure to arbitrary inputs in a computationally efficient manner. This work describes the application of the nonlinear modal modeling test and identification process on two industrial structures. For each structure, the linear modal analysis and the nonlinear identification are presented. A truth test is conducted on each structure, the results of which are compared to corresponding simulation results using the linear and nonlinear modal models. The nonlinear modal models are shown to better match the measured responses of both structures.

Keywords: nonlinear dynamics, system identification, modal modeling, structural dynamics, industrial applications

1 Introduction

Essential to the robust design of structures is a model that accurately captures the relevant dynamics in its service environments. Historically, linear models have been used in this regard to great success. They are computationally efficient and can be updated via dynamic properties identified from modal tests [1]. However, if there are significant nonlinear physics active during service environments, then linear modelling may not be able to sufficiently replicate the true response of the structure, detracting from their utility in qualification decisions. Thus, there are circumstance where a nonlinear structural dynamics model is required. There are many frameworks for nonlinear modeling, testing, and identification, such as nonlinear normal modes [2] and spectral manifolds [3], but this work focuses on nonlinear modal models (NLMMs) [4, 5]. NLMMs are comprised of single degree of freedom (SDOF) oscillators which each represent a mode of vibration of the structure and have nonlinear springs and dampers that attach the modal mass to ground. As has been demonstrated in [6, 7] and will be shown in this work, NLMMs are able to capture the amplitude-dependent behavior of nonlinear, industrial structures and can be used to replicate the response to arbitrary inputs in a computationally efficient manner.

This work presents two case studies where NLMMs were applied to industrial structures. The first was a structure with mounted components and bolted joints, and an NLMM was desired that could capture the amplitude-dependent response within a specified bandwidth. The second case study utilized a structure with multiple bolted joints, and the dynamic behavior of a specific mode was desired up to approximately 300gs. Each case study is introduced in greater detail where the testing and NLMM identification is described. Each NLMM is then evaluated on its ability to match the responses obtained via time simulation to those measured from corresponding truth tests on each structure.

The remainder of this work is organized as follows. Section 2 describes NLMMs in greater detail including assumptions and limitations. The methods for testing and identification of NLMMs are presented in Section 3. The two industrial case studies where NLMMs were used to capture their nonlinear dynamics are discussed in Sections 4.1 and 4.2. A summary of these works is provided in Section 5.

2 Nonlinear Modal Models

Nonlinear modal models are the same as their linear counterparts except for additional amplitude-dependent stiffness and damping elements for modes deemed to be nonlinear, see Fig. 1. The number of modes retained in the NLMM is determined by the bandwidth of interest. The physical and modal coordinates of the structure are related through:

$$\{x(t)\} = \mathbf{\Phi}\{q(t)\} \tag{1}$$
$$\{q(t)\} = \mathbf{\Phi}^{+}\{x(t)\} \tag{2}$$

†Sandia National Laboratories is a multimission laboratory managed and operated by National Technology & Engineering Solutions of Sandia, LLC, a wholly owned subsidiary of Honeywell International Inc., for the U.S. Department of Energy's National Nuclear Security Administration under contract DE-NA0003525.

with $\{x(t)\}$ and $\{q(t)\}$ the displacement of the structure in physical and modal coordinates, respectively, $\boldsymbol{\Phi}$ is the mass-normalized mode shape matrix, and the "+" superscript is the Moore-Penrose Pseudo-inverse. Similarly, the excitation force in modal $\{f_q(t)\}$ and physical $\{f(t)\}$ coordinates are related through the following transformation:

$$\{f_q(t)\} = \boldsymbol{\Phi}^{\mathrm{T}}\{f(t)\} \tag{3}$$

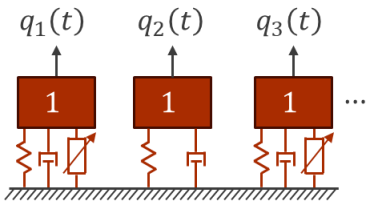

Fig. 1 Nonlinear modal model

Each mode j can be described by the following equation of motion:

$$\ddot{q}_j(t) + c_{0,j}\dot{q}_j(t) + k_{0,j}q_j(t) + f_{r,nl,j}\left(q_j(t), \dot{q}_j(t)\right) = f_{q,j}(t) \tag{4}$$

where $k_{0,j}$ and $c_{0,j}$ are the linear spring and damper coefficients, respectively, and are defined by the corresponding natural frequency, $\omega_{n,j}$, and damping ratio, ζ_j:

$$k_{0,j} = \omega_{n,j}^2 \tag{5}$$

$$c_{0,j} = 2\zeta_j\omega_{n,j} \tag{6}$$

The nonlinear modal restoring force is $f_{r,nl,j}\left(q_j(t), \dot{q}_j(t)\right)$ and is the subject of the nonlinear identification (see Section 3.3). This force combines all of the nonlinear effects of mode j into a single force, so this approach to nonlinear structural dynamics obtains the overall amplitude-dependent stiffness and damping forces as opposed to identifying specific physics associated with a particular nonlinear source.

The work presented herein makes two assumptions. The first is that the mode shapes do not change with amplitude. This allows the use of the linear mode shape matrix to be used to transform between physical and modal coordinates. Second, the modes are assumed to be uncoupled. In other words, the response of one mode does not influence or excite the response of another.

3 Test Methods and Identification

This section discusses the test and identification methods for case studies presented in this work. The identification of the NLMM for both case studies utilized data from sine beat excitation [6] (Section 3.1), but nonlinear force appropriation [2, 8] (Section 3.2) was conducted on the structure for Case Study 2 to explore a potential modal interaction.

3.1 Sine Beats

Sine beat excitation [6] utilizes a modal shaker to concentrate a transient force in the bandwidth around a mode of interest, see Fig. 2. It is created by modulating a sinewave by an amplitude windowing function $a(t)$:

$$v(t) = a(t)\sin(\omega_c t) \tag{7}$$

where $v(t)$ is the sine beat and ω_c is the center frequency. Note that $v(t)$ is the voltage signal that is sent to the shaker and is not the force applied to the structure; the resulting force is a function of both the shaker and structure dynamics. The peak of $V(\omega)$ (the Fourier Transform of $v(t)$) occurs at ω_c and the width of its main lobe is directly related to $a(t)$ [6]. Since $a(t)$ is a user-defined function, the input energy of a sine beat can be customized to provide forcing of a single, targeted mode while minimally exciting the others.

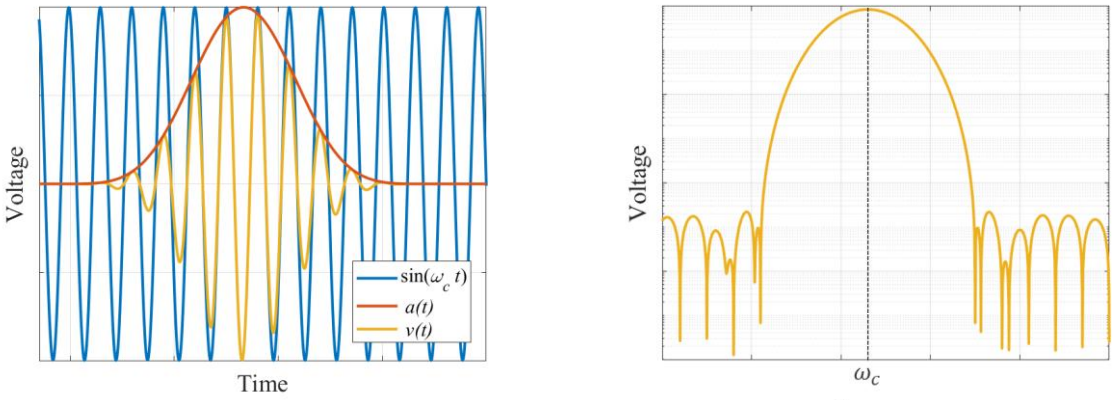

(a) (b)

Fig. 2 Sine beat in (a) time domain and (b) frequency domain

In this work, each nonlinear mode was individually excited using sine beats. The frequency ω_c was selected as the linear natural frequency of the target mode. The windowing function $a(t)$ was a Blackman-Harris window whose parameters were selected such that either (1) the first local minima on either side of the peak in $V(\omega_c)$ occurred at adjacent modes, or (2) the width of the main lobe in $V(\omega)$ encompassed the same bandwidth as the imaginary part of the target mode in the drive point frequency response function (FRF).

3.2 Nonlinear Force Appropriation

Nonlinear force appropriation (NFA) testing (also known as phase resonance testing) is a technique that utilizes closed loop control to maintain a structure at phase resonance while the amplitude of excitation is slowly increased [2, 8]. For this work, phase resonance was defined as 90 degrees relative phase between the drive point acceleration response and excitation force at the fundamental frequency; in other words, the primary phase resonance [9, 10] was achieved at each excitation level. Fig. 3 shows a block diagram of the NFA test technique. A voltage sinewave of constant amplitude V and frequency ω is sent to a modal shaker which induces a force $f(t)$ on the structure. The corresponding drive point acceleration $\ddot{x}_{dp}(t)$ and $f(t)$ are measured by the Phase-Locked-Loop (PLL) controller. The PLL controller adjusts ω based on the computed error between 90 degrees and the relative phase between $\ddot{x}_{dp}(t)$ and $f(t)$. The updated voltage signal is generated and sent to the shaker. This cycle continues until phase resonance is achieved, and data is collected from all of the accelerometers on the structure. The energy input to the structure is then increased by increasing V, and the above process repeats capturing the entire backbone of the structure over a chosen amplitude range.

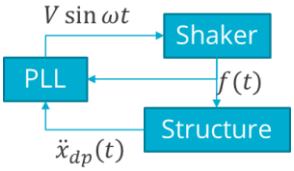

Fig. 3 Force appropriation block diagram

This technique characterizes a single mode from low (ideally linear) levels up to a desired high energy level. While not performed in this work, the data used from NFA tests can be used for nonlinear modal model identification. Additionally, modal interactions are more obviously excited and observed with NFA testing than sine beats. This testing technique was conducted in Case Study 2 to show a potential modal interaction (see Section 4.2.2).

3.3 Nonlinear Modal Model Identification

The general process for NLMM identification is shown in Fig. 4. It begins with a linear modal test of the structure from which the linear natural frequencies, damping ratios, and mode shapes are extracted. The nonlinear modes of the structure are detected through comparing the FRFs from experiments where the structure was impacted at multiple force levels. Modes where the FRFs significantly shifted were deemed nonlinear. A signification shift is a subjective

measure and will depend on the application. Sections 4.1 and 4.2 describe the nonlinear mode selection process for the corresponding case studies.

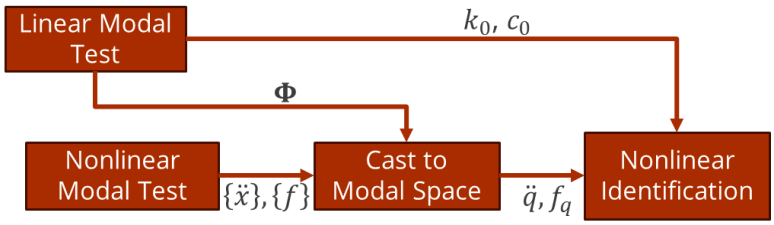

Fig. 4 NLMM identification procedure

The nonlinear modal test is then conducted for each nonlinear mode. For the case studies in this work, this comprised the sine beats. The result of this experiment are the measured accelerations $\{\ddot{x}\}$ measured in physical coordinates, and the excitation force $\{f\}$. Only single input excitation was used for this work, so only the element of $\{f\}$ corresponding to the drive point DOF is non-zero. These measurements are then cast to modal space using Eqs. (2) and (3). The identification is performed on the mode of interest.

The nonlinear identification process described below is the same as that described in [6] and is similar to the process presented in [11]. The mode of interest is now described by Eq. (4). The linear stiffness and damping coefficients (k_0 and c_0) are computed from Eqs. (5) and (6) using the results from the linear modal test. The modal velocity and displacement are determined via numerical integration of $\ddot{q}(t)$. Therefore, the only unknown is the nonlinear restoring force $f_{r,nl}\big(q(t), \dot{q}(t)\big)$ which is assumed to be the sum the nonlinear stiffness and damping restoring forces ($f_{r,nl,s}(q)$ and $f_{r,nl,d}(\dot{q})$, respectively):

$$f_{r,nl}\big(q(t), \dot{q}(t)\big) = f_{r,nl,s}(q) + f_{r,nl,d}(\dot{q}) \tag{8}$$

While $f_{r,nl,s}(q)$ and $f_{r,nl,d}(\dot{q})$ can be parameterized in many ways, symmetric polynomials were used for both case studies described in this work:

$$f_{r,nl,s}(q) = \sum_{n=1}^{N_s} k_n q|q|^{n-1} \tag{9}$$

$$f_{r,nl,d}(\dot{q}) = \sum_{n=1}^{N_d} c_n \dot{q}|\dot{q}|^{n-1} \tag{10}$$

N_s and N_d are the maximum selected polynomial order for $f_{r,nl,s}(q)$ and $f_{r,nl,d}(\dot{q})$, respectively, and k_n and c_n are the associated polynomial coefficients. The absolute values of q and $\dot{q}$ are used to ensure that the identified restoring forces are symmetric, an assumption made for all nonlinear modes in both case studies.

Eqs (8) through (10) are substituted into Eq. (4). The result is rearranged and cast to the frequency domain to yield

$$\begin{bmatrix} \mathcal{F}(q|q|) & \dots & \mathcal{F}(q|q|^{N_s-1}) & \mathcal{F}(\dot{q}|\dot{q}|) & \dots & \mathcal{F}(\dot{q}|\dot{q}|^{N_d-1}) \end{bmatrix} \begin{bmatrix} k_1 \\ \vdots \\ k_{N_s} \\ c_1 \\ \vdots \\ c_{N_d} \end{bmatrix} = \big[\mathcal{F}\big(f_q - \ddot{q} - c_0\dot{q} - k_0 q\big)\big] \tag{11}$$

where $\mathcal{F}(\ \ )$ is the Fourier Transform and represent columns of data in the above matrices. The polynomial coefficients for the nonlinear restoring forces can be solved for in a least-squares since using:

$$\begin{bmatrix} k_1 \\ \vdots \\ k_{N_s} \\ c_1 \\ \vdots \\ c_{N_d} \end{bmatrix} = [\mathcal{F}(q|q|) \quad \dots \quad \mathcal{F}(q|q|^{N_s-1}) \quad \mathcal{F}(\dot{q}|\dot{q}|) \quad \dots \quad \mathcal{F}(\dot{q}|\dot{q}|^{N_d-1})]^{+}\left[\mathcal{F}\left(f_q - \ddot{q} - c_0\dot{q} - k_0 q\right)\right] \tag{12}$$

where the "+" is the Moore-Penrose Pseudoinverse. The parameterized $f_{r,nl}\left(q(t), \dot{q}(t)\right)$ is now identified for the mode of interest. Note that data from multiple tests can be stacked within each matrix on the right-hand-side of Eq. (12). For both of the case studies in this work, sine beats at multiple levels were conducted and the corresponding data were all used to fit the parameters.

This entire process is repeated for each mode of interest that is deemed nonlinear. All modes (linear and nonlinear) are then concatenated into a nonlinear modal model of the entire structure:

$$\mathbf{I}\{\ddot{q}(t)\} + \mathbf{C_0}\{\dot{q}(t)\} + \mathbf{K_0}\{q(t)\} + \left\{f_{r,nl}\left(\{q(t)\}, \left\{\dot{q(t)}\right\}\right)\right\} = \left\{f_q(t)\right\} \tag{13}$$

where $\mathbf{I}$ is the identity matrix, $\mathbf{C_0}$ is a diagonal linear damping matrix with entries of individual $c_{0,j}$ for each mode j, $\mathbf{K_0}$ is a diagonal linear stiffness matrix with entries of individual $k_{0,j}$ for each mode j, and $\left\{f_{r,nl}\left(\{q(t)\}, \left\{\dot{q(t)}\right\}\right)\right\}$ is the vector of nonlinear restoring forces defined by Eq. (8) for each nonlinear mode. In this formulation, row j of Eq. (13) corresponds to Eq (4) for each mode j.

The response of the entire structure, $\{x(t)\}$, to an arbitrary force $\{f(t)\}$ can be simulated using Eq. (13) by first casting the force in physical coordinates to modal coordinates using Eq. (3). With assumed modal displacement and velocity initial conditions and $\left\{f_q(t)\right\}$, Eq. (13) is used to obtain $\{q(t)\}$ via time simulation. These modal responses are then cast back to physical coordinates, $\{x(t)\}$, using Eq. (1). These $\{x(t)\}$ are the simulated response of the structure using the identified NLMM and incorporate the amplitude-dependent stiffness and damping due to the nonlinear modes.

Generating an explicit nonlinear model of an industrial structure where the physics are exactly captured is difficult to update via system identification experiments. Moreover, the computational cost to simulate the response of a structure to arbitrary inputs with this model is prohibitively expensive. Conversely, the NLMM is highly computationally efficient and, while not exactly modelling the underlying physics, is able to capture the amplitude dependence of the stiffness and damping of each nonlinear mode. Therefore, the NLMM approach is attractive for industrial applications.

4 Case Studies: Industrial Applications of the NLMM

In Sections 4.1 and 4.2, the NLMM identification process described in Section 3.3 was implemented on two industrial structures. After conducting linear modal analysis, sine beats were used to excite each structure to high levels. The NLMMs were then identified, and truth tests conducted. The accuracy of the NLMM was evaluated by comparing its predicted response to the truth test forcing to that measured from the experiment. Additionally, for Case Study 2, NFA testing was conducted to evaluate a potential modal interaction. This latter result was not used explicitly in the NLMM identification for this case but is shown to demonstrate that modal interactions occur in industry. It also motivates future research to incorporate this nonlinear behavior into the NLMM process.

4.1 Case Study 1

The objective of Cast Study 1 was to conduct nonlinear system identification of the structure and obtain a NLMM. The test article is shown in Fig. 5 and is comprised of many components mounted to a case. The source of the nonlinearities arises from the interfaces between the components and the case.

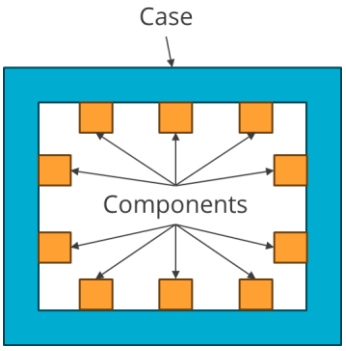

Fig. 5 Case Study 1 test article

4.1.1 NLMM Identification

There were 18 modes within the bandwidth of interest, six rigid and twelve elastic. The rigid body modes were computed using the companion finite element model and the elastic modes were extracted from linear modal testing, see Fig. 6. Fig. 6a compares the measured principle complex mode indicator function (CMIF) from the linear modal tests with that resynthesized from the identified linear modal properties. Fig. 6b shows the auto Modal Assurance Criterion for the extracted linear modes. These results indicate that the linear modal properties accurately represent the low-level dynamics of the test article and that the identified modes are independent. This latter aspect is critical to achieving advantageous conditioning on $\boldsymbol{\Phi}^{+}$ when casting the nonlinear modal testing results from physical to modal coordinates.

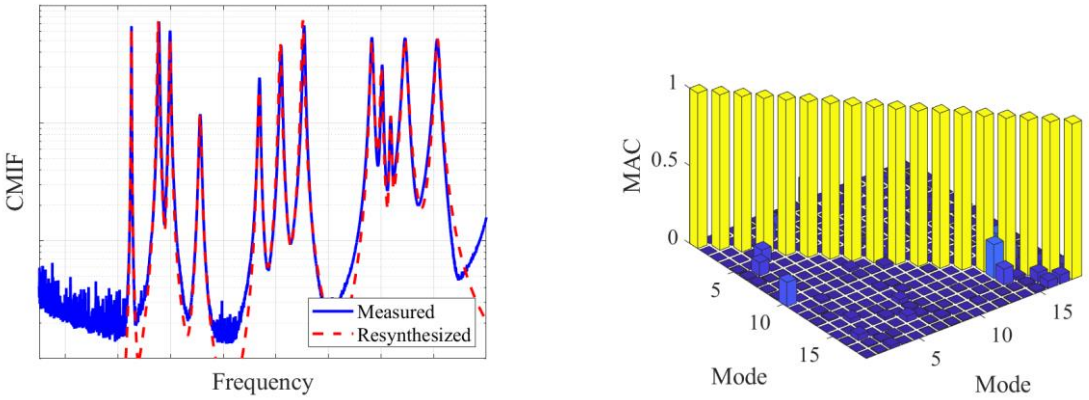

(a) (b)

Fig. 6 Case Study 1 linear modal test results; (a) measured vs resynthesized CMIF and (b) auto-MAC

Through multi-level hammer impact testing, modes 7, 11, 12, 13, and 15 showed the largest shifts in the measured FRFs; no objective measure was used in the determination (e.g., a damping change threshold) but was left to the judgement of the author. Fig. 7 shows the CMIF overlays in the bandwidth around the selected nonlinear modes from three different hammer impact levels. Note that all modes show an increase in damping and decrease in frequency.

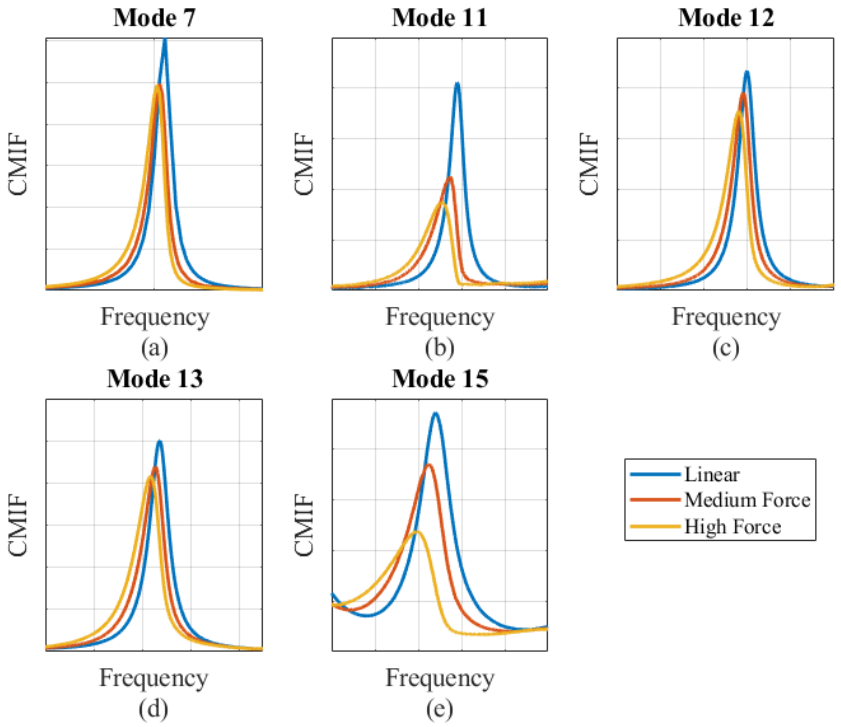

Fig. 7 Case Study 1 CMIFs from multiple input force levels showing nonlinearity of these modes

Sine beats were used to excite each of the nonlinear modes up to as high of level as possible. The limiting factor in this case was the electrical output of the amplifier that powered the shaker. The identification was performed per Section 3.3 with $N_s = N_d = 3$ for all five nonlinear modes. Cubic polynomials were selected as a balance between obtaining accurate representation of the nonlinear restoring force and minimizing the model order to preclude over-fitting. To evaluate the accuracy of the identified NLMM of the test article, a truth test was conducted. This was a sine-sweep whose amplitude vs frequency was shaped in order to maximize the response of the structure at each mode. The measured force from this truth test was cast to modal space and used in the NLMM simulation of the test article per Eq. (13). The resulting modal responses were expanded back to physical coordinates in order to compare against the accelerations measured during the truth test.

Fig. 8 shows select time history and frequency domain results from measurements on two of the components of the test article. Along with the measured and NLMM results, the accelerations predicted by a purely linear model are also shown to demonstrate the improvement achieved with the NLMM. In the frequency domain results, dashed vertical lines indicate the frequencies of the nonlinear modes. In the bandwidth around linear modes, all three data sets agree, confirming the decision to maintain these modes as linear. Conversely, the NLMM is shown to better match the measured results in the vicinity of the nonlinear modes. In some instances, the linear model over-predicts the response by a factor of 2, but the NLMM is able to accurately match the measured response.

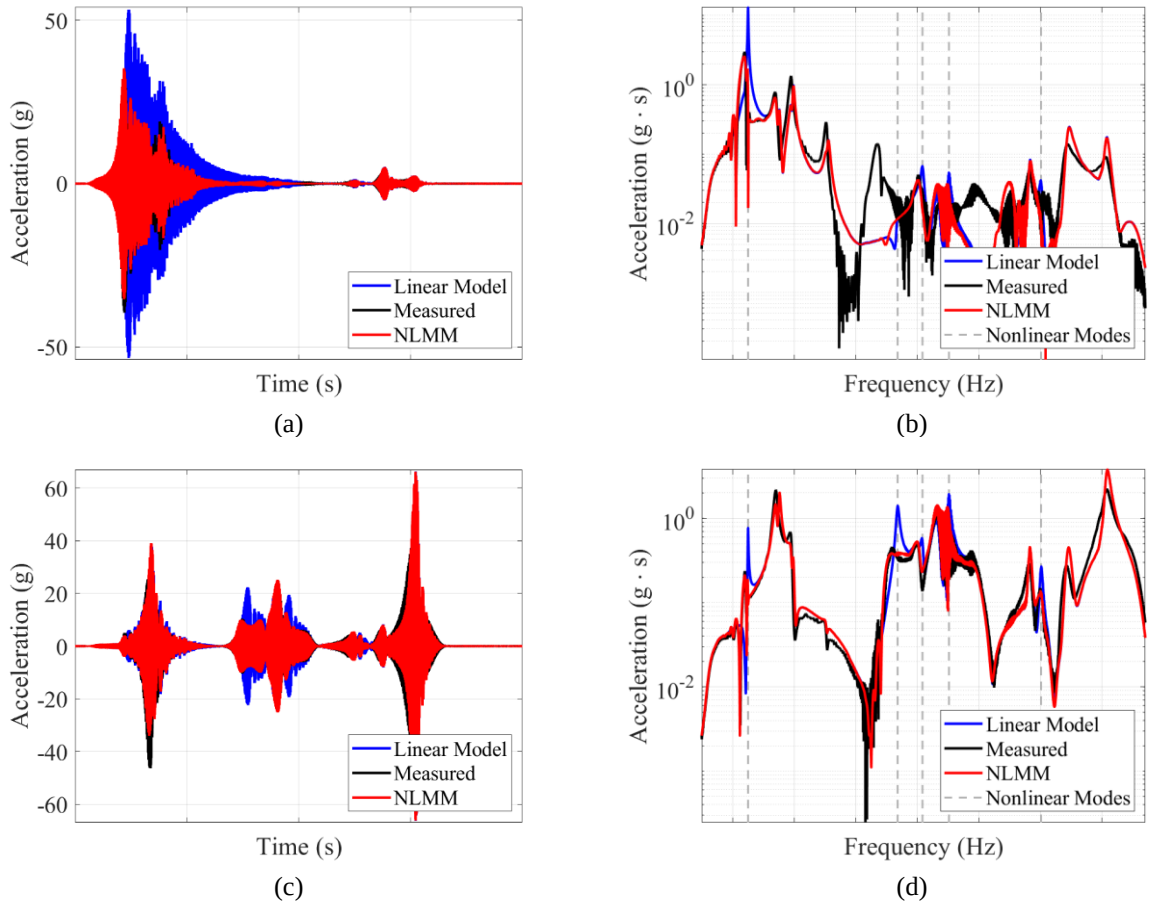

Fig. 8 NLMM vs measurements from truth test, Case Study 1; (a) time history and (b) frequency domain response of component 1 and (c) time history and (d) frequency domain response of component 2. Black data is the measurement from the truth test, the red data is the simulation result from the NLMM, the blue data is the linear simulation result, and the dashed vertical gray lines ((b) and (d) only) indicate the frequencies of the nonlinear modes

4.2 Case Study 2

The objective of Case Study 2 was to characterize the nonlinear damping of a single mode of interest up to a high level (300 g at the drive point). The structure was tested in free-free boundary conditions and is shown in Fig. 9. The mode of interest exercised shear motion in the indicated joint between the fixture and the plate. Sine beats were conducted to perform the NLMM identification of the mode of interest (Section 4.2.1). NFA testing was also conducted to investigate a potential modal interaction (Section 4.2.2).

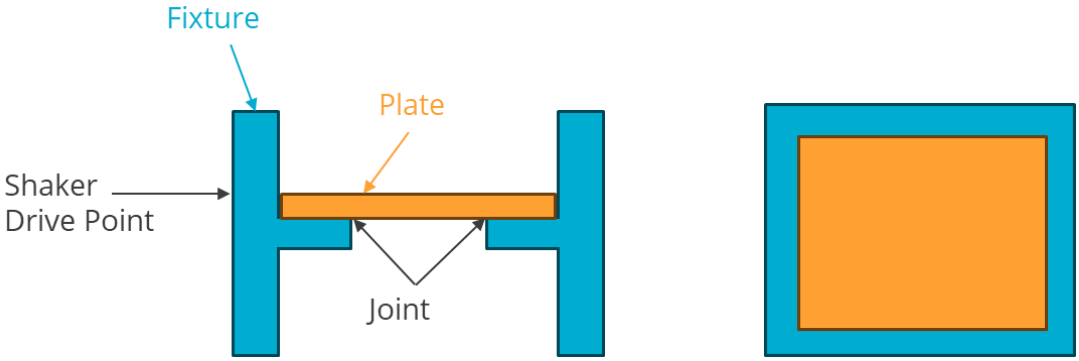

Fig. 9 Case Study 2 test article (a) cross-section and (b) top view

Unlike Case Study 1, there is only one mode of interest for Case Study 2 where an NLMM was desired. However, linear modal testing was still required over a larger bandwidth of interest in order to get the linear modal parameters for the mode of interest as well as $\boldsymbol{\Phi}$ to transform between physical and modal coordinates.

Linear modal testing was conducted via low force level hammer impacts. Fig. 10 shows the results. The linear modal parameters were used to resynthesize the FRF matrix from which a multi-reference CMIF was computed. This resynthesized CMIF was compared to the corresponding measured CMIF. Fig. 10a shows the principle single value from the measured and resynthesized CMIF. Twenty elastic modes are active within the bandwidth, and the mode of interest (mode 10) is marked with an arrow. The high correspondence between measured and resynthesized data indicates that the extracted linear modal parameters match well the linear dynamics of the test article. Additionally, Fig. 10b shows the auto-MAC of the experimentally extracted mode shapes (along with six rigid body modes taken from the FEM of the test article). The identified modes are reasonably independent, but there are some mode pairs which have higher than ideal values (e.g., mode 21 and 22 have a MAC value of 0.6). Nonetheless, the mode shape matrix has a condition number of approximately 9 which deemed the modes acceptably independent for this work.

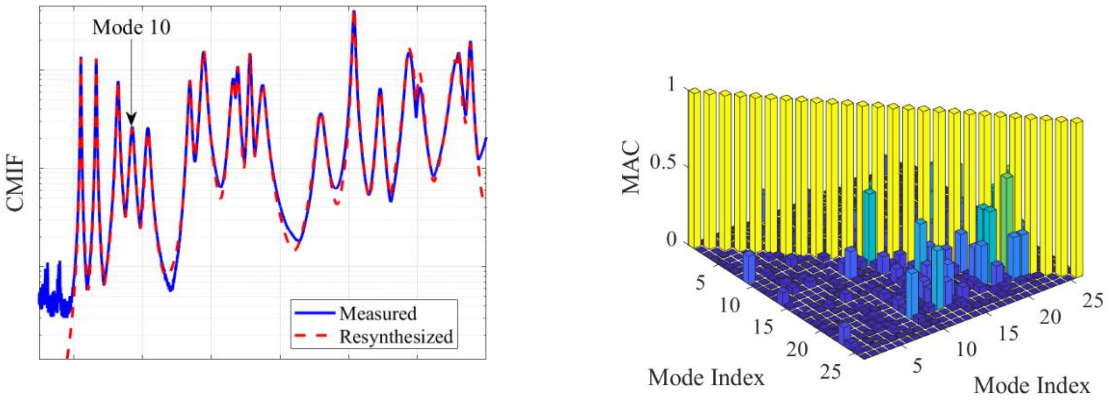

Fig. 10 Case Study 2 linear modal test results; (a) measured (solid lines) vs resynthesized (dashed lines) CMIF and (b) auto-MAC

Note that the underlying linear dynamics of the test article shifted throughout the test series as indicted by low-level testing conducted between all tests, see Fig. 11. The mode of interest is marked with a black arrow. The test sequence was as follows: (1) low-level hammer impacts, (2) NFA, and (3) sine beats. The change in the drive point FRF between the hammer and NFA tests shows the effect of adding the shaker, and the shift between NFA and sine beats shows the change in underlying linear dynamics after achieving high level excitation.

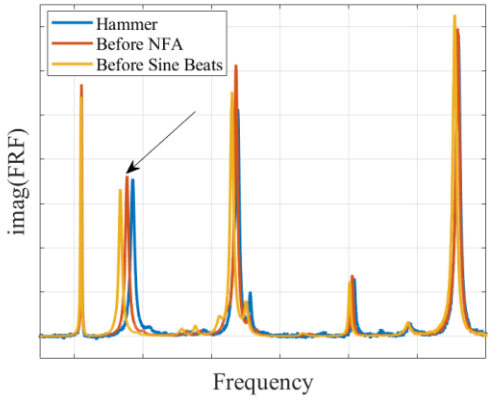

Fig. 11 Drive point FRF comparison at various stages throughout Case Study 2 testing

Due to the apparent change in linear dynamics, three sets of linear modal properties were fit and used throughout the CS2 work. The first set is the baseline extracted from the low-level hammer taps. A set of linear properties were used to process data from each of the high-level tests. These were constructed from the baseline set, but the natural frequencies, damping ratios, and shapes were updated for the modes well excited from the shaker drive point (i.e., the modes well excited from Fig. 11). The largest differences in linear modal properties for the target mode were between the baseline and the sine beat sets. The differences in the natural frequency and damping ratio of the target mode were approximately 7% and 20%, respectively. The corresponding MAC value for the target mode shape was 0.78. This highlights a practical consideration for nonlinear system characterization in that the underlying linear properties can change throughout the test series. This was accounted for in this work by assigning linear modal properties for each test type which best describes the corresponding underlying linear dynamics.

4.2.1 Nonlinear Modal Model Identification

The NLMM was constructed with 26 modes (six rigid and 20 elastic) where only mode 10 was assumed nonlinear since the objective was to obtain an NLMM of only the target mode. Given the high response levels achieved from the sine beat testing, the order of the nonlinear stiffness and damping restoring force polynomials were $N_s = N_d = 5$ for mode 10. Other modes of the structure were known to be nonlinear, so the evaluation of the NLMM was conducted using narrow-band excitation to minimize the nonlinear effects of the other modes. Thus, the accuracy of the NLMM was assessed using the measurements from the highest-level sine beat. Fig. 12 shows the results for two acceleration DOFs. The first is the drive point (Fig. 12a and b) and the second is the DOF with the largest value in the target mode shape (referred to as the "max DOF" shown in Fig. 12c and d). These figures compare the measured acceleration response with those computed via linear and NLMM simulation.

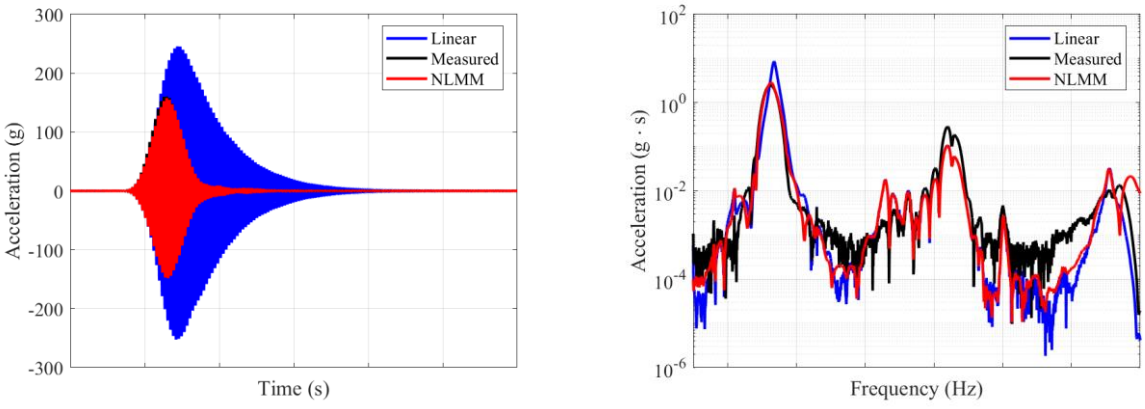

(a) (b)

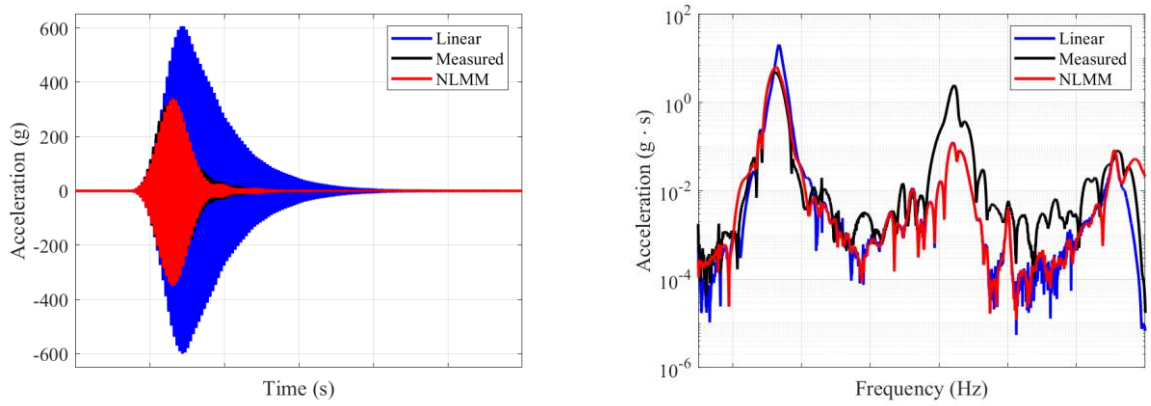

(c) (d)

Fig. 12 NLMM results; drive point acceleration in (a) time domain and (b) frequency domain, and the acceleration response of the DOF with the largest shape in the target mode (i.e., "max DOF") in (c) time domain and (d) frequency domain

In both responses, the NLMM matches the measured result well and is a significant improvement in accuracy over the linear model; the linear model over-predicts the peak response by factors of 1.5 and 1.8, respectively, for the measured drive point and max DOF accelerations. Fig. 12d shows that the max DOF has a large second harmonic compared to that shown in Fig. 12b for the drive point. The NLMM does not correctly capture the harmonic at the former DOF, indicating that one of the fundamental assumptions is not fully satisfied by the dynamics of the test article and/or that the chosen model form is not able to adequately capture the response. Based on the results discussed in Section 4.2.2, part of the reason for this higher-frequency discrepancy between measured and NLMM response is that the mode of interest (mode 10) is interacting with a higher-frequency mode.

4.2.2 NFA Results

An NFA test was conducted initially as an additional measure to characterize the mode of interest. However, during the test, a potential modal interaction between modes 10 and 18 was observed. Seventy excitation levels (i.e., values of V from Fig. 3) were selected, and phase resonance was achieved at each. In the plots that follow, the abscissa is labeled with "Excitation Index," corresponding to the shaker voltage indices when phase resonance was achieved.

Fig. 13 shows a subset of the NFA results. The magnitudes of the first 5 harmonics of max DOF are shown in Fig. 13a. The dashed lines correspond to the even harmonics which are shown to be significant with respect to the fundamental frequency. The linear natural frequency of mode 18 is approximately twice that of mode 10, so the large second harmonic indicates a potential for a modal interaction. The measured accelerations from the NFA test were cast to modal space. The magnitudes of all harmonics of all modes which surpass 50% of that of the fundamental component of the mode of interest (mode 10) are plotted in Fig. 13b. Only the second harmonic of mode 18 exceeds this threshold and even exceeds the amplitude of the fundamental component of the mode 10. Thus mode 18 is well excited and is comprised on mainly of the second harmonic. Furthermore, the MAC between the linear shape of mode 18 and the operational deflection shape of the second harmonic is shown in are plotted in Fig. 13c. The minimum MAC value is 90, indicating a high correlation between these two shapes and that the second harmonic is deforming in the shape of mode 18. No other linear mode shape had a MAC value larger than 30. Lastly, shakers can produce a second harmonic in force through their own nonlinear electrodynamics [12], so there is potential that, given the high amplitude forcing, mode 18 is being driven by the nonlinearity of the shaker. Fig. 13d shows the imaginary part of the drive point FRF with modes 10 and 18 indicated. This FRF shows that mode 18 is poorly excited by the drive location, and therefore it is unlikely to be driven to such high amplitudes via any shaker nonlinearity.

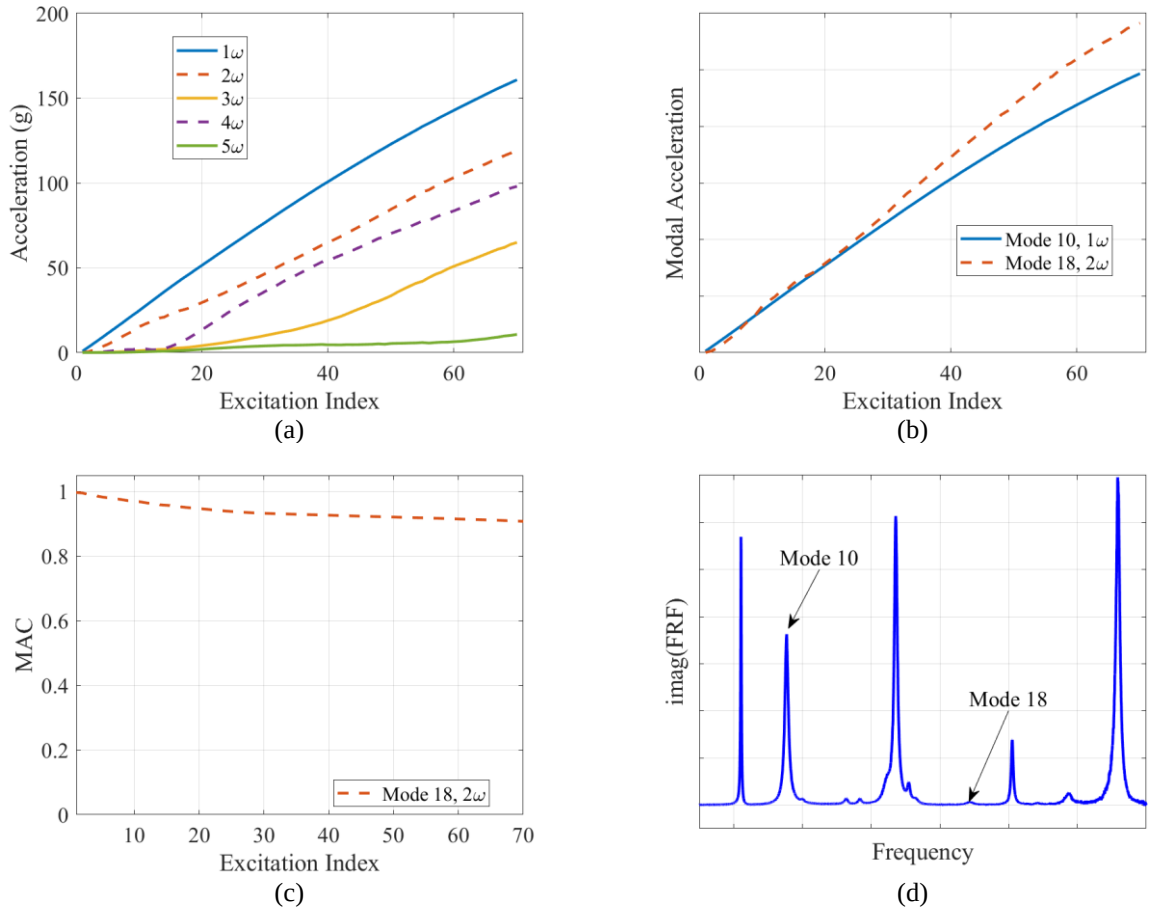

Fig. 13 NFA results showing a modal interaction between modes 10 and 18; (a) max DOF frequency content; (b) significant frequency content for all modes; (c) MAC between mode 18 and the deflection shape of the second harmonic; and (d) imaginary part of the drive point FRF showing that mode 18 is not well excited by the shaker

These plots indicate that during the NFA test of mode 10 a large second harmonic that deformed in the shape of mode 18 was active in the measured response. Additionally, the amplitude of mode 18 is equal to or greater than that of the mode targeted by the NFA test. It was also shown that shaker nonlinearity was not the likely source of mode 18 excitation. Therefore, these results indicate that a modal interaction occurred between modes 10 and 18, driven by the nonlinear physics activated by the joint of interest. These results corroborate the observation from Fig. 12d that the NLMM is unable to replicate the second harmonic response of max DOF in the sine beat because modal interactions violate one of the underlying assumptions of the NLMM. This motivates future work to include additional nonlinear forcing terms in the NLMM formulation to include modal interactions as this work has shown that this nonlinear phenomenon can occur in industrial structures.

5 Summary

Two case studies from industry were presented where nonlinear modal modelling was used first to identify the nonlinear modes of each structure and then to predict the full-field response to an arbitrary excitation force. The main sources of nonlinearity in both case studies were bolted joints. The objective for Case Study 1 was to capture all the nonlinear modes within a bandwidth of interest. The aim for Case Study 2 was only to identify and develop a nonlinear modal model for a single mode of interest up to high levels of response. In both cases, the nonlinear modal model was shown to generally replicate the measured response of the structures well and proved to be an improvement over a strictly linear approach.

This work showed that nonlinear modal models were able to accurately capture the response of two industrial structures in a computationally efficient manner. This technique assumes that the modes are uncoupled and that they do not interact. For Case Study 2, the nonlinear modal model simulation less accurately replicated the structural

response at the second harmonic of the mode of interest. Further investigation via nonlinear force appropriation testing of the mode of interest revealed a modal interaction: the nonlinearity activated in the mode of interest generated a second harmonic which excited a higher frequency mode. Therefore, the decreased accuracy of the nonlinear modal model simulation results at this higher frequency is attributed to the structure violating an underlying assumption of the nonlinear modal modeling process. This motivates the future work of developing identification techniques to incorporate this type of behavior into the nonlinear modal modeling process.

Acknowledgements
Sandia National Laboratories is a multi-mission laboratory managed and operated by National Technology & Engineering Solutions of Sandia, LLC (NTESS), a wholly owned subsidiary of Honeywell International Inc., for the U.S. Department of Energy's National Nuclear Security Administration (DOE/NNSA) under contract DE-NA0003525. This written work is authored by an employee of NTESS. The employee, not NTESS, owns the right, title and interest in and to the written work and is responsible for its contents. Any subjective views or opinions that might be expressed in the written work do not necessarily represent the views of the U.S. Government. The publisher acknowledges that the U.S. Government retains a non-exclusive, paid-up, irrevocable, world-wide license to publish or reproduce the published form of this written work or allow others to do so, for U.S. Government purposes. The DOE will provide public access to results of federally sponsored research in accordance with the DOE Public Access Plan.

This paper describes objective technical results and analysis. Any subjective views or opinions that might be expressed in the paper do not necessarily represent the views of the U.S. Department of Energy or the United States Government.

6 References

[1] D. J. Ewins, Modal Testing: Theory, Practice, and Application, 2 ed., Bognor Regis, West Sussex, England: John Wiley & Sons, 2009.

[2] M. Peeters, G. Kerschen and J. Golinval, "Dynamic testing of nonlinear vibrating structures using nonlinear normal modes," *Journal of Sound and Vibration,* vol. 330, pp. 486-509, 2011.

[3] G. Haller and S. Ponsioen, "Nonlinear normal modes and spectral submanifolds: existence, uniqueness and use in model reduction," *Nonlinear Dynamics,* vol. 86, pp. 1493-1534, 2016.

[4] R. L. Mayes, B. R. Pacini and D. R. Roettgen, "A modal model to simulate typical structural dynamic nonlinearity," in *Dynamics of Coupled Structures, Volume 4: Proceedings of the 34th IMAC, A Conference and Exposition on Structural Dynamics 2016*, Orlando, FL, 2016.

[5] M. F. Platten, J. R. Wright, G. Dimitriadis and J. E. Cooper, "Identification of multi-degree of freedom non-linear systems using an extended modal space model," *Mechanical Systems and Signal Processing,* vol. 23, no. 1, pp. 8-29, 2009.

[6] B. R. Pacini, R. L. Mayes, B. C. Owens and R. A. Schultz, "Nonlinear finite element model updating, part I: experimental techniques and nonlinear modal model parameter extraction," in *Dynamics of Coupled Structures, Volume 4: Proceedings of the 35th IMAC, A Conference and Exposition on Structural Dynamics 2017*, Garden Grove, CA, 2017.

[7] B. C. Owens, R. A. Schultz, B. R. Pacini and R. L. Mayes, "Nonlinear Finite Element Model Updating, Part II: Implementation and Simulation," in *Dynamics of Coupled Structures, Volume 4: Proceedings of the 35th IMAC, A Conference and Exposition on Structural Dynamics 2017*, Garden Grove, CA, 2017.

[8] S. Peter and R. I. Leine, "Excitation power quantities in phase resonance testing of nonlinear systems with phase-locked-loop excitation," *Mechanical Systems and Signal Processing,* vol. 96, pp. 139-158, 2017.

[9] M. Volvert and G. Kerschen, "Phase resonance nonlinear modes of mechanical systems," *Journal of Sound and Vibration,* vol. 511, 2021.

[10] M. Volvert and G. Kerschen, "Resonant phase lags of a Duffing oscillator," *International Journal of Non-Linear Mechanics,* vol. 146, 2022.

[11] T. Breunung, L. Cilenti, J. You and B. Balachandran, "Robust Identification of Nonlinear Oscillators from Frequency Response Data," in *Nonlinear Structures & Systems, Volume 1. SEM 2023. Conference Proceedings of the Society for Experimental Mechanics Series*, Austin, TX, 2023.

[12] G. R. Tomlinson, "Force distortion in resonance testing of structures with electro-dynamic vibration exciters," *Journal of Sound and Vibration,* vol. 63, no. 3, pp. 337-350, 1979.

[13] G. Kerschen, K. Worden, A. F. Vakakis and J.-C. Golinval, "Past, present and future of nonlinear system identification in structural dynamics," *Mechanical systems and signal processing,* vol. 20, no. 3, pp. 505-592, 2006.

[14] J.-P. Noël and G. Kerschen, "Nonlinear system identification in structural dynamics: 10 more years of progress," *Mechanical Systems and Signal Processing ,* vol. 83, pp. 2-35, 2017.